High-speed imaging of cathode spots in a Vacuum Arc Thruster

Etienne Michaux, Stéphane Mazouffre

High-speed imaging of cathode spots in a Vacuum Arc Thruster

IEPC-2024-291

Presented at the 38th International Electric Propulsion Conference, Toulouse, France
June 23-28, 2024

E. Michaux* , J. Julien† and S. Mazouffre‡
Institut de Combustion, Aérothermique, Réactivité et Environnement (ICARE) - CNRS, Orléans, 45000, France

The apparent movement of plasma emission sites across the cathode surface of a 30 W vacuum arc thruster is examined using high-speed imaging. Images captured at a frame rate of 450,000 fps reveal the temporal evolution of the cathode spot distribution over the course of a single current pulse. Films were recorded using two different cathode materials: titanium and copper. A comparison with the discharge current shows a locally high current density, on the order of 10^9 A/m^2. Quantitative analysis on clustering of cathode spots, and the mapping of their trajectory over the cathode surface offer insights into the cathode erosion dynamics.

*PhD Student, ICARE–CNRS, etienne.michaux@cnrs-orleans.fr
†Graduate Student, ICARE–CNRS/IPSA, jeremie.julien@ipsa.fr
‡Research Director, ICARE–CNRS, stephane.mazouffre@cnrs-orleans.fr

I. Introduction

The vacuum arc thruster (VAT) is an electric space thruster that creates an electrical arc. Contrary to what happens at atmospheric pressure, in vacuum there is no medium to ionize. The electrode where the lowest potential is applied, the cathode, is vaporized and ionized. The ejected plasma generates a thrust in the opposite direction. The VAT is a simple and robust thruster, thus a good choice for micro-propulsion applications. In addition, the storage density is high and there is no need for any fluid management system or tank.

However, the vacuum arc is a complex and highly dynamic phenomenon. On rather small time scales, plasma properties change and the plasma emission sites move over the cathode surface [1]. Their study is then difficult, and some aspects of the vacuum arc behavior remain unclear despite more than 70 years of research effort [2,3]. Most recent research works highlight the fractal nature of cathode spots,[4] which are the plasma emission sites at the cathode surface. This nature is reflected both in the way the spots are distributed on the cathode surface, and in the voltage fluctuations noise at the electrodes [5]. In other words, the vacuum arc shows a high complexity both in the spatial and in the temporal domain.

In the context of VATs, the arc is pulsed with a short duration in order to avoid thermal issues. A study on the arc dynamics is then of high importance. In particular, knowledge on the cathode spots distribution throughout the discharge duration is of major interest when it comes to engineering considerations. In fact, VATs suffer from performance limitations due to the random nature of the cathode erosion. In this study, the time evolution of cathode spots that cover the surface is investigated by means of high-speed imaging. Measurements are performed with a 30-W VAT that has the particularity of operating a very high current, in the magnitude of kiloamperes. The clustering mechanism of plasma emission sites is observed in the context of a high-current vacuum arc, as well as the spots current density for two different cathode materials. Ultimately, the propagation speed of the spot structure is determined and conclusions are drawn.

II. Experimental arrangement

A. The Plasma Jet Pack

The Plasma Jet Pack (PJP) is a high-current Vacuum Arc Thruster (VAT) developed by the COMAT french company. Several PJP versions have been developed to date, for different needs and different satellite integrations[6]The PJP under study is the H2020 version, designed to be easily dismountable which allows testing of different electrode configurations. In particular, this version can be equipped with cathodes made out of different materials. The PJP generates a high-current vacuum arc through the cyclic discharges of a capacitor bank. The repetition frequency can reach 2 Hz at maximum, for a power consumption of 30 W. The cathode to anode voltage is continuously set to 250 V. A triggering system applies a few kV pulse on the cathode surface for 1 µs. This pulse allows ignition of the plasma through an explosive process[7]. The cathode material is locally vaporized and ionized, on surface regions called cathode spots. After the trigger is switched-off, the arc is forced to propagate to the anode through the existing metal vapor. This second arc discharge allows roughly 2.5 to 4 kA to flow between the two electrodes with the present configuration, depending on the cathode material. Overall, the energy released over 30 µs into one single PJP discharge reaches more or less 3 J. Measurements presented in this work have been conducted with a copper anode and two different cathode materials: titanium and copper. Averaged PJP discharge current waveforms (I_d) are given in Fig. 1a, over the whole dataset, for titanium and copper cathodes. Despite slight differences in the maximum current from one pulse to an other, the temporal evolution of the discharge current remains the same for a given cathode material. In brief the I_d waveforms are highly reproducible for a given cathode material.

Figure 1b shows the front view of a laboratory version of the PJP. The 4-legs electrode is the annular copper anode. The cathode corresponds to the grey center-mounted hollow cylinder. The latter is screwed onto a copper plate directly wired to the capacitor bank. The gap in the axial direction between the cathode and the anode is approximately 1 cm. The trigger electrode is a tiny metal tip placed exactly on the thruster axis of symmetry and separated from the cathode with the central insulator. The picture inside the green frame in Fig. 1b is a long exposure photograph of the cathode surface during a discharge [8]. The cathode spots are here the bright branches that develop on the cathode surface. The central insulator is dark in this picture as the spots develop solely on the cathode surface. The PJP target performance and characteristics are given in Table 1 for the inclined reader.

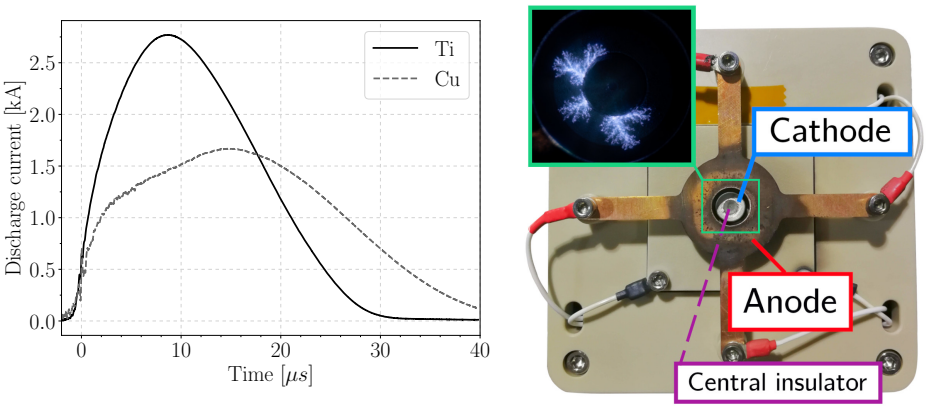

(a) Typical PJP discharge current waveform during one pulse

(b) PJP thruster: front view. In the green frame (top left), long exposure photograph shows the cathode spot distribution on the PJP cathode surface during a discharge.

Figure 1: PJP thruster front view and averaged discharge current waveform.

Table 1: PJP thruster target performance and characteristics.

Power	0-30	W
Thrust to power	10	µN/W
Average thrust at 30 W	300	µN
Specific impulse	2500	s
Total impulse	400	Ns
Overall mass	1	kg
Overall volume	1	U

B. EPIC-2 vacuum chamber

Experiments have been performed in the EPIC-2 vacuum chamber. This tank is a stainless steel cylinder 54 cm in diameter and 104 cm in length, for an approximate capacity of 240 L. Two 2200 L/s (N_2) magnetically levitated Edwards STP-iS2207 are placed on top of the chamber (see Fig. 2a). Those pumps evacuated through a 110 m^3/h dry primary pump (Edwards GV110), permit to keep a background pressure of 10^{-6} mbar during thruster operation. The pressure is monitored with a Pfeiffer PBR260 Pirani/Payard-Alpert pressure gauge.

EPIC-2 is also equipped with several electrical feedthroughs, for both in-situ diagnostics and thruster power supply. Those feedthroughs are mostly composed of BNC or SubD connectors. Two Kodial (Borosilicate 7056) glass windows allow the visual inspection of the thruster during operation. Inside the chamber, the PJP is mounted on a square fixed to a plate, the latter being screwed on rails. This mounting allows adjustments of the distance to the windows or to instruments, depending on the experiment to be performed.

C. High-speed imaging

It was shown in ref .8 that the spot distribution strongly varies from one pulse to an other. This chaotic nature of vacuum arc [4,5] requires examination on a pulse-by-pulse basis. Therefore, the use of a high-speed camera is necessary for studying the spots motion dynamics. In this context, the Phantom TMX7510 camera was the best available option. It features a CMOS sensor with an acquisition frequency of up to 1.7 million frames per second (fps). However, at this rate, the image resolution has to be lowered to 256x32 px. To ensure all the cathode surface is contained in the image and that no spot initiates out of the frame, the image resolution is set in this study to 256x128 px. This resolution leads to an acquisition frequency of 450,000 fps, which represents roughly one picture every 2.2 µs. With these settings, 13 photographs are captured

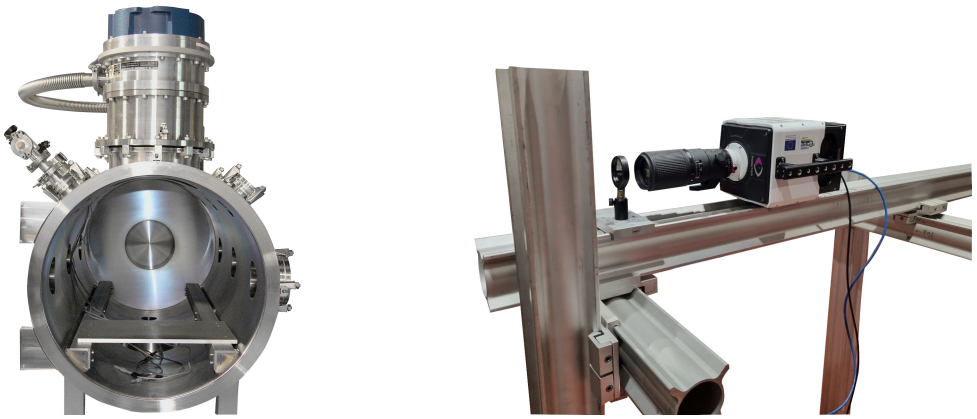

(a) Inside view of the chamber, through the open door. The rails and the thruster support plate are here placed inside.

(b) Assembly of the TMX7510 with the 200 mm lens. A neutral density filter is placed on the stand.

Figure 2: PJP thruster front view and averaged discharge current waveform.

throughout a single PJP discharge.

The camera captures footage of the thruster from outside the chamber, through a quartz window. To enhance observational capabilities, a Nikon 200 mm lens is mounted on the camera. This enable zooming on the cathode surface, so that it fills the entire camera field of view. For the same reason, the PJP is placed 30 cm away from the window, which is the closest possible position. Overall, the camera lens is positioned 90 cm away from the cathode, on a stainless steel stand as depicted in Fig. 2b. Due to the large amount of light emitted during the discharges, 2 neutral density filters are installed upstream of the lenses. These filters have a respective optical density of 1 and 2, ensuring that the camera sensor is not saturated. Such saturation would result in a loss of information in the acquired images.

III. Methodology

In order to compare this study with previous results obtained with this VAT [8], a series of 30 pulses is performed prior to measurements. These pulses are used to remove the oxide layer formed on the cathode, which modifies the behavior of the vacuum arc [9–11]. To ensure the best possible level of detail, focus is achieved by setting the camera's exposure time to 10 ms, its maximum. This increases the image brightness when no arc is triggered, thus facilitating manual focusing. A calibration image is taken after focusing, and used as a reference for automatic cathode edge detection as it will be explained later. For video acquisition, the exposure time is reduced to 1.9 µs, which is as close as possible to the acquisition period of 2.2 µs. This limits the loss of information between 2 images. The camera is triggered by the PJP trigger signal, the associated discharge current is recorded on the oscilloscope. 150 associations of videos and discharge current were recorded for titanium, and 50 for copper. This difference is due to the thermal expansion issue on copper and pollution of the insulators, which leads to thruster damage in its current configuration [12]. Example of a video taken with a titanium cathode is shown in Fig 3.

Data analysis algorithms are based here on OpenCV. This computer vision library incorporates functions for image processing. Hence, it enables the automatic treatment of a large volume of images. In our study, OpenCV is used to determine cathode edges on all the videos. Due to the geometry of the PJP H2020, an arc can form on the side of the cathode or present anodic modes. Although these phenomena are fairly rare, these luminous areas must not be confused with cathode spots, as this could distort the result when calculating the mean surface covered by the spots or their propagation speed. The cathode edge determination is then an important prerequisite for further rigorous analysis.

For a pixel to be identified as a cathode spot, its brightness must exceed a given threshold. This threshold is set according to the cathode material, as the elements emits at different wavelengths, with different intensities. For example, the threshold for titanium has been set at 96% of the maximum pixel intensity (240/255), while for copper it's 88%. These values are obviously not absolute, and are empirically

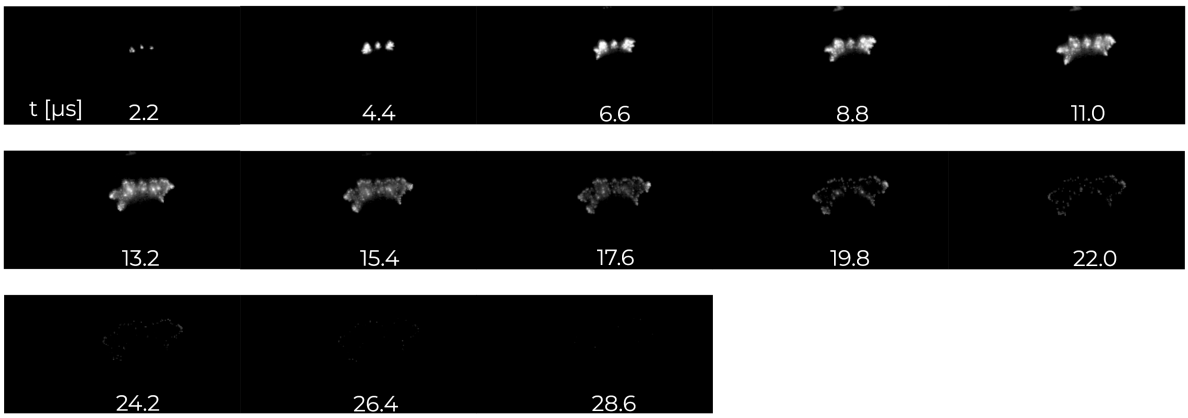

Figure 3: 13 frames composing a video. Ti cathode.

adapted to our datasets and optical equipment. It is important to correctly set this threshold since the spots produce a lot of light, illuminating the cathode surface. The spots are a primary source of light and the cathode itself is a secondary source, not an active plasma emission site. Reflected light should not be counted as a cathode spot, to reduce inaccuracies on the results.

IV. Results

A. Spot surface

On the whole, see Fig. 3, the spots tend to cluster near the center at the beginning of the discharge. This was to be expected, as the HV trigger tip is located at the center of the cathode central insulator (see Fig. 1b). The breakdown is therefore initiated where the electric field is the strongest: i.e close to the trigger tip. As explained in section A, once the trigger is switched off the arc migrates toward the main anode. The latter is circular in shape, and its diameter is larger than the outer diameter of the cathode. The electric field E is therefore radial on the picture, leading to a predominantly radial propagation of the cathode spots as the arc is attracted to the outside edge. This does not exclude the possibility for the spots to propagate in a tangential direction. The phenomenon is indeed seen in Fig. 3. It should also be noted that in this figure, the spots propagate in the top half section of the picture. The preferred side is in fact determined by the breakdown initation area, as the spots successively ignite close to the already existing ones [13,14]. The preferred propagation area changes then from one pulse to an other.

On another matter, the total surface covered by the spots shows a significant evolution during the discharge. As spots propagate towards the outside edge, they cover an increasingly larger surface. Figure 4 presents a comparison between the discharge current and the evolution of the covered area as a function of time, for the video exemplified in Fig. 3. The 13 points between 0 and 28 µs on the graph correspond to the frames composing Fig 3. The maximum surface is reached when the discharge current reaches its maximum, then it decreases and falls back to zero. We can see that the 2 curves exhibit a high degree of similarity, which is observed consistently across all recorded videos. The 2.2 µs offset between the two curves in Fig 4 originates in the time taken by the camera to acquire an image (exposure time).

The correlation between the discharge current $I_d(t)$ and the surface covered in time $S(t)$ can be quantified by determining the Spearman rank-order correlation coefficient r_s. This coefficient ranges from -1 to +1: +1 indicating an exact monotonic correlation, -1 an inverse monotonic correlation, and 0 no correlation. Its calculation is relatively simple and well implemented in python libraries as it is widely used in different research areas [15,16]. In our example, $r_s = 0.95$ which means a strong correlation between $I_d(t)$ and $S(t)$. The mean values of r_s for the videos of each material dataset are shown in Table. 2. On average, $r_s = 0.948$ for titanium, while for copper it decreases 0.483. The standard deviation for Ti is 0.05 and 0.3 for Cu. It is worth mentioning that in the Cu dataset, many $I_d(t)$ curves show noise and bumps as exemplified in Fig. 1a. This noise has already been observed in previous studies and is due to the metal deposition on the PJP insulating surfaces. Copper deposits much more easily on the insulating ceramics, resulting in short circuits. Part of

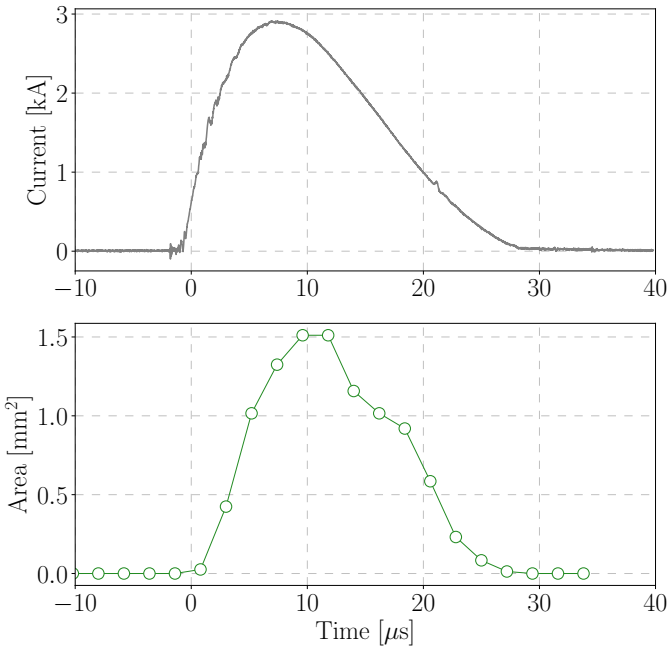

Figure 4: Comparison between the discharge current (top) and the evolution of the spot surface (bottom) for the example video.

the current coming from the capacitor bank passes through these conductive layers and $I_d(t)$ is disturbed. This disturbance of $I_d(t)$ for copper largely explains the smaller r_s for this material. Table 2 also shows the average surface covered per image, and the average maximum surface covered during pulses. It can be seen that titanium covers more surface in average, which is consistent with the observations in ref. [8].

Table 2: Average values of surface covered, maximum surface and spearman coefficient. Values are taken over 150 pulses for Ti and 50 pulses for Cu.

Material	Ti	Cu
Surface [mm^2]	0.345	0.267
Maximum surface [mm^2]	1.124	0.508
r_s	0.948	0.483

B. Spot clustering

Another interesting phenomenon to look at when studying the cathode spots is the clustering dynamics. In fact, the spots captured by the camera consist of numerous smaller spots, each of them on the scale of tens of µm. Siemroth et al. [17] propose to classify spots into 3 categories, depending on their size. Ranging from the smallest to the largest, first are the microspots, each approximately tens of µm in size. Then are the macrospots, observable through a camera. Ultimately, group spots are clusters of macrospots. The group spots can vary in size. Each macrospot can sustain a limited current density, which depends on the cathode material. When the maximum current density is reached, another spot is initiated and may or may not cluster with the previous one [2,3]. In high-current vacuum arcs, a large number of macrospots are simultaneously active [13,18]. It is therefore interesting to look at the spot clustering in the context of a PJP discharge.

For this purpose, a depth-first search (DFS) algorithm has been implemented. This algorithm is generally

used for exploring tree data structures [19]. The DFS initiates at a root node and explores as far as possible along each branch before backtracking [20]. In our case, it starts at a pixel and explores neighboring pixels with a brightness greater or equal to the imposed threshold as defined in section III. When a darker pixel is encountered, the algorithm returns to the previous pixel and explores its neighbors again. Therefore, the algorithm recursively explores clustered spots structures. Subsequently, each group spot is assigned a unique identifier, facilitating the mapping and counting of these clusters. Figure 5 shows the group spots as identified by the DFS algorithm on 3 different images of the video exemplified in Fig 3 (Ti cathode). The different groups are highlighted in different colors. Note that on the 8.8 µs and the 17.6 µs images, the algorithm detects more group spots than there are colors in the palette. Different clusters can therefore be highlighted in a similar color. It is noticeable that at the beginning of the discharge the spots are clustered in large groups. As the discharge continues, they split and move further apart. The spots are therefore smaller and more numerous. In the case of copper (see Fig. 6), the dynamics is less rich. The spots remain small and clustered around the central insulator. They form fewer branches and remain farther apart during all the discharge. All of this is consistent with observations on long-exposure photographs taken in ref.8.

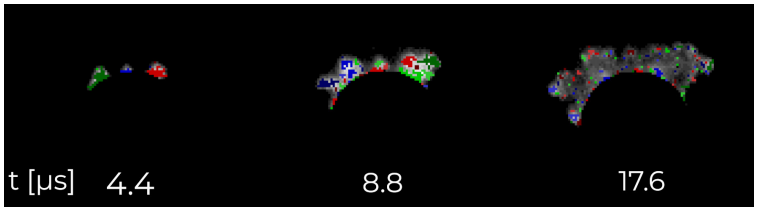

Figure 5: Group spot recognition with the DFS algorithm. Ti cathode.

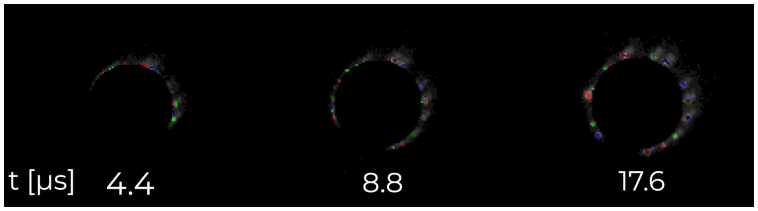

Figure 6: Group spot recognition with the DFS algorithm. Cu cathode.

The average size and number of groups spots during a PJP discharge is given in table 3, as well as the average maximum size of the group spots. Values are given in pixels to ease visualization. Time of occurence indicates when the group spots are the largest during the discharge. On average for titanium, group spots are both more numerous and larger. One can note that the larger spots form at the beginning of the discharge, whereas for copper they tend to form at half time or at the end. This can be explained by the less rich spot dynamics when it comes to the copper vacuum arc. The standard deviation of the Cu spot surface is indeed smaller. It is then more difficult to conclude on a real mechanism of maximum spot clustering at a given time for the copper cathode. It is yet known that the apparent spot motion on the cathode surface follows a random walk behavior, more particularly a self avoiding walk. This means that an extinguished spot has little chance of being active again, at least in a short period of time. Overall, this means that large clusters of spots tend to split without ever reforming, as observed on Titanium. One thing should be considered here. The titanium cathode presents large clusters starting from the center and moving outwards while disintegrating, whereas copper shows small clusters distributed around the center. In both cases, over the whole pulse, cathode erosion occurs predominantly close to the central insulator. The cathode is therefore not eroded evenly across its entire radius.

C. Current density

Figure 7 shows the evolution of current density as a function of time on the video exemplified in Fig. 3. This figure is obtained by dividing $I_d(t)$ by $S(t)$ (see Fig. 4). One can note 2 periods with high current density j at the beginning and the end of the discharge. Indeed, due to the identification method, uncertainty on the surface computation is large for these two instants. At the start, the spots are tightly grouped as explained

Table 3: Group spot properties for Ti and Cu.

Material	Ti	Cu
Size [px]	2.84 ± 0.44	2.28 ± 0.12
Size [mm^2]	1.83×10^{-2}	1.47×10^{-2}
Maximum size [px]	51.24 ± 22.15	10.91 ± 2.58
Maximum size [mm^2]	0.33	0.07
Time of occurrence [μs]	4.4	15.4
Number of groups	37	18

in the previous section. This tends to overestimate j because several spots are present per pixel. At the end of the discharge, the spots are scattered and not very bright. The optical arrangement of neutral density filters prevents these spots from being seen clearly, as their brightness falls below the threshold. This results in an underestimation of the surface area and, consequently, an overestimation of j.

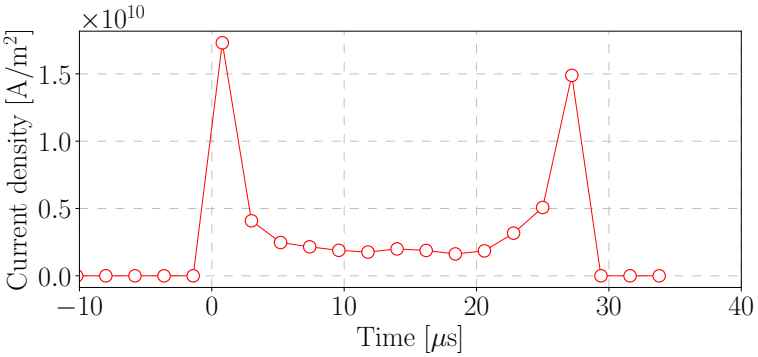

Figure 7: Evolution of the current density over time. Example video, Ti cathode.

If we disregard these 2 peaks, j remains stable around 2.5×10^9 A/m^2. The correlation between $I_d(t)$ and $S(t)$ has already been discussed in section A, it is then natural that current density should be relatively stable as current and surface evolve together. We can therefore calculate the average current density by taking the average current and dividing it by the average spot surface covered during the pulse. Results are given in table 4. References in literature [17,21] give a value of 5×10^9 A/m^2 according to the "large spot" model. This model predates the fractal spot model, developed in the early 2000s to better describe the cathode spot behavior [2,4]. Here, because of the image resolution, the fractal model cannot be directly applied to our observations. Current density is then underestimated due to overestimation of the spot surface. In addition, direct observation of the cathode spots by optical means inherently overestimate their surface [22,23]. The dense, rapidly expanding plasma from the spots can show a brightness almost equal to the one of the spot, within a certain radius. More recent studies suggest that the spot current density would be closer to 10^{11} A/m^2, based on the ecton model[18] and advanced techniques such as pulsed laser absorption photography [24] or pulsed laser interferometry [25].

Table 4: Average current density for the 2 materials.

Material	Ti	Cu
Discharge current [A]	1.48×10^3	1.03×10^3
Spot current density [A/m^2]	4.3×10^9	3.8×10^9

Ultimately, the fractal model gives another perspective on the quest to determine the exact current density in cathode spots. They are self-similar and thus seem, with each new technological progress, to be composed of ever-smaller fragments. The question of the real spot current density is then still open and, in

the end, is rather abstract.

D. Spot velocity

The propagation speed of the spots defines the capacity of the arc to erode the cathode. Combined with the observation of spots clustering, it gives important information on the dynamics of cathode erosion throughout a single PJP pulse. Implementing a tracking algorithm is quite complex here, given the random nature of spot motion and the low resolution of the image. However, successful results have been obtained with a modified particle tracking velocimetry (PTV) algorithm. PTV algorithms usually embed motion prediction models based on fluid mechanics physics in order to help the tracking from one frame to the other. Still, a reduced weight of this model on the detection algorithm allows to track semi-stochastic movement, with the condition of a fine tuning of the other tracking parameters. Here, we have specified an average spot size to search for, to aid spot detection. These sizes correspond to the average group spot sizes given in Table 3. In doing so, we mainly track the clusters and fewer spots are identified, reducing the number of detection errors. This choice was made to ease the tracking as the pictures are in gray-scale, the algorithm could therefore only analyze luminosity gradients and not the red-green-blue matrices.

Result of the tracking for the video shown in Fig. 3 is shown in Fig. 8. The background picture is a sum of all the frames composing the video, making it analogous to a long-exposure photograph. The displayed lines are the trajectories of the different group spots tracked on this video. Trajectories are colorized according to their respective average speed (norm of the velocity vector), the crosses symbolize the exact location where the spots have been identified. As seen previously, trajectories can be tangential or radial, with no apparent correlation between the propagation direction and the speed. As an example, two orange trajectories with speed of around 60 m/s are observed on the left of the figure despite that they are respectively almost purely radial and tangential. A looping trajectory is observed at coordinates [150,45], showing the robustness of the algorithm when it comes to identify quasi-stochastic movement. However, we note that most clusters appear to propagate in relatively straight lines. In particular, we remark the tracking of a relatively slow spot on the left of the figure. This spot is identified over 9 consecutive images and show no abrupt change of direction throughout its course. This could indicate a macro effect of spot clustering, meaning that spots tend to lose their stochastic behavior when they cluster and show a preferential propagation direction. On the other hand, it may also be linked to the camera low spatial and temporal resolution compared to the spot propagation phenomenon, making it impossible to see small variations in the trajectory.

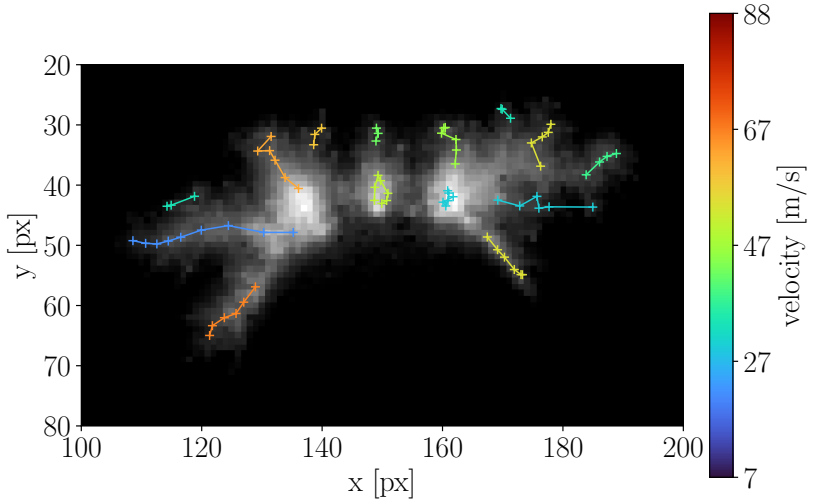

Figure 8: Tracking of the spots. Data taken from video shown in Fig. 3, Ti cathode.

Average velocities and the associated standard deviations for the 2 materials are given in Table. 5. The differences between the 2 materials lie in all the observations made so far: titanium shows richer dynamics than copper, which is naturally reflected in the propagation speed. It should be noted that the speeds presented here are consistent with the data available in the literature[3,26] despite the different experimental arrangement.

Table 5: Average values of propagation speed and associated standard deviation.

Material	Ti	Cu
$\bar{v}$ [m/s]	38.5	12.8
Standard deviation	10.4	3.3

V. Conclusion

For the same energy released in the discharge, titanium and copper show very different cathode spot dynamics. Titanium spots tend to form large clusters which split later during discharge. They propagate rapidly in the radial direction, but can also propagate in a tangent way. When the PJP is equipped with a copper cathode, the spots remain grouped close to the central insulator for all the discharge duration, despite the latter lasting longer. They propagate mainly in the tangent direction, and are way slower than titanium cathode spots. For the two cathode materials, although the dynamics is different, the result is quite the same from an engineering perspective: cathode erosion occurs mainly on the inner edge. This can be life-limiting, as the propellant is not used optimally over the entire cathode surface.

The direct observation of the emission surface over time shows the existence of great similarity with the discharge current waveform. This is reflected in the calculation of the average current density per spot, which is around $4 \times 10^9\,\mathrm{A/m^2}$ for the 2 materials. However this value can be discussed due to the fractal nature of vacuum arc cathode spots, which makes it difficult to quantify the unit size of an emission cell. This study show the average behavior of a vacuum arc thruster, as a whole, taking data over many pulses. Accurate characterization of each pulse is a major challenge, due to the inherently stochastic nature of the vacuum arc.

Acknowledgments

Authors would like to thank C. Chauveau and F. Halter for the high-speed camera as well as S. Iseni and M. Idir for the high quality optics.

References

[1]JE Daalder. Random walk of cathode arc spots in vacuum. Journal of Physics D: Applied Physics, 16(1):17, 1983.

[2]A Anders. Cathodic arcs: from fractal spots to energetic condensation, volume 50. Springer, 2008.

[3]II Beilis. Plasma and Spot Phenomena in Electrical Arcs, volume 113. Springer Nature, 2020.

[4]A Anders. The fractal nature of vacuum arc cathode spots. IEEE Transactions on Plasma Science, 33(5):1456–1464, 2005.

[5]A Anders, EM Oks, and GY Yushkov. Cathodic arcs: Fractal voltage and cohesive energy rule. Applied Physics Letters, 86(21):211503, 2005.

[6]A Blanchet, L Herrero, L Voisin, B Pilloy, and D Courteville. Plasma jet pack technology for nano-microsatellites. In 36th International Electric Propulsion Conference, 2019.

[7]GA Mesyats. Ecton or electron avalanche from metal. Physics-Uspekhi, 38(6):567, 1995.

[8]E Michaux, AE Vinci, and S Mazouffre. Fractal dimension of cathode spots in a high-current vacuum arc thruster. Vacuum, page 112286, 2023.

[9]K Oh, D Kalanov, and A Anders. High-resolution observation of cathode spots in a magnetically steered vacuum arc plasma source. Plasma Sources Science and Technology, 30(9):095005, 2021.

[10]K Oh, D Kalanov, P Birtel, and A Anders. High-resolution observation of cathodic arc spots in a magnetically steered arc plasma source in low pressure argon, nitrogen, and oxygen atmospheres. Journal of Applied Physics, 130(18):183304, 2021.

[11]M Golizadeh, A Anders, F Mendez Martin, S Kolozsvári, and R Franz. Insights into surface modification and erosion of multi-element arc cathodes using a novel multilayer cathode design. Journal of Applied Physics, 127(11):113301, 2020.

[12]E Michaux and S Mazouffre. Time-of-flight measurements in the jet of a high-current vacuum arc thruster. Aerospace, 10(12):1011, 2023.

[13]B Juttner. Nanosecond displacement times of arc cathode spots in vacuum. IEEE transactions on plasma science, 27(4):836–844, 1999.

[14]II Beilis. Vacuum arc cathode spot theory: history and evolution of the mechanisms. IEEE Transactions on Plasma Science, 47(8):3412–3433, 2019.

[15]J Hauke and T Kossowski. Comparison of values of pearson's and spearman's correlation coefficients on the same sets of data. Quaestiones geographicae, 30(2):87–93, 2011.

[16]J De Winter, S Gosling, and J Potter. Comparing the pearson and spearman correlation coefficients across distributions and sample sizes: A tutorial using simulations and empirical data. Psychological methods, 21(3):273, 2016.

[17]P Siemroth, T Schulke, and T Witke. Investigation of cathode spots and plasma formation of vacuum arcs by high speed microscopy and spectroscopy. IEEE Transactions on Plasma Science, 25(4):571–579, 1997.

[18]GA Mesyats and SA Barengolts. The cathode spot of a high-current vacuum arc as a multiecton phenomenon. IEEE transactions on plasma science, 29(5):704–707, 2001.

[19]TH Cormen, CE Leiserson, RL Rivest, and C Stein. Introduction to algorithms. MIT press, 2022.

[20]MT Goodrich and R Tamassia. Algorithm design: foundations, analysis, and internet examples. John Wiley & Sons, 2001.

[21]VI Rakhovsky. State of the art of physical models of vacuum arc cathode spots. IEEE transactions on plasma science, 15(5):481–487, 1987.

[22]S Anders, A Anders, and B Juttner. Brightness distribution and current density of vacuum arc cathode spots. Journal of Physics D: Applied Physics, 25(11):1591, 1992.

[23]E Hantzsche, B Juttner, and G Ziegenhagen. Why vacuum arc cathode spots can appear larger than they are. IEEE transactions on plasma science, 23(1):55–64, 1995.

[24]A Anders, S Anders, B Juttner, W Botticher, H Luck, and G Schroder. Pulsed dye laser diagnostics of vacuum arc cathode spots. IEEE transactions on plasma science, 20(4):466–472, 1992.

[25]N Vogel. The cathode spot plasma in low-current air and vacuum break arcs. Journal of Physics D: Applied Physics, 26(10):1655, 1993.

[26]II Beilis, B Sagi, V Zhitomirsky, and RL Boxman. Cathode spot motion in a vacuum arc with a long roof-shaped cathode under magnetic field. Journal of Applied Physics, 117(23), 2015.